Self-Assembly of the Perfluoroalkyl-Alkane $F_{14}H_{20}$ in Ultrathin Films

Ahmed Mourran,*,†,‡ Bernd Tartsch,† Marat Gallyamov,†,§ Sergei Magonov,‖ Denitza Lambreva,⊥ Boris I. Ostrovskii,⊥ Igor P. Dolbnya,¶ Wim H. de Jeu,⊥ and Martin Moeller*,†,‡

Organische Chemie III, Makromolekulare Chemie, Universität Ulm, Albert-Einstein-Allee 11, 89069 Ulm, Germany, Digital Instruments, Robin Hill Road 112, California 93117, FOM-Institute for Atomic and Molecular Physics, Kruislaan 407, 1098 SJ Amsterdam, The Netherlands, and DUBBLE CRG, ESRF, BP 220, 38043 Grenoble, France

Received July 30, 2004. In Final Form: November 9, 2004

Scanning force microscopy on monomolecular films of eicosylperfluorotetradecane, $F(CF_2)_{14}(CH_2)_{20}H$, on mica, silicon oxide, or water revealed spontaneous organization to well-defined nanoscopic ribbon and spiral or toroidal superstructures. Whether ribbons or nanospirals were formed depended on the solvent from which the molecular monofilm was cast. Ribbons were observed when a hydrocarbon or a perfluorocarbon solvent was used, e.g., decalin or perfluorodecalin. When the compound, however, was deposited from nonselective hexafluoroxylene, the molecules assembled into spirals of defined size. The spirals/toroids transformed to ribbons when exposed either to decalin or perfluorodecalin vapor, and the ribbons transformed to toroids when exposed to hexafluoroxylene vapor. These changes could be observed in situ. Scanning force microscopy yielded an identical height and width for the bands forming the spirals and for the parallel flat ribbons. X-ray reflectivity yielded a height of 3.61 ± 0.05 nm, again identical for both morphologies. Yet, the length of the extended $F(CF_2)_{14}(CH_2)_{20}H$ molecule, i.e., 4.65 nm, exceeds the layer thickness obtained from X-ray reflectometry. It is, however, consistent with an arrangement where the fluorinated chains are oriented normal to the surface layer and where the alkyl segments are tilted with a 122° angle between the two segments. Within the plane defined by the tilt, this angle allows a dense packing of the alkyl segments compensating for the larger cross-section of the fluorocarbon segment. The tilt plane defines an "easy" direction along which the monolayer structure can preserve order. In the plane perpendicular to this axis, long-range ordered dense packing of the alkyl chains is not possible. Incommensurable packing can in principle explain the finite and regular width of the ribbons and the stepwise turn in the spirals.

1. Introduction

Semifluorinated alkanes, i.e., with a perfluorinated chain segment, consist of two incompatible subunits that segregate into distinct domains in the melt as well as in the crystalline state.[1−4,14] In this respect they resemble block copolymers, but with the peculiarity that they can be prepared as uniform samples without polydispersity in molecular weight.[14] Structural ordering of such compounds is, however, controlled not only by the strong incompatibility of the constituting segments but also by the fact that the van der Waals cross-section of the flexible hydrocarbon segment is 25−30% smaller than that of the rather rigid perfluorinated segment. The antagonistic nature of the two building units and the mismatch in cross-section between the perfluoro and the perhydro alkyl tail result in distinct superstructure formation. Indeed, dependent on the block length and the temperature, the competition between ordering of the hydrocarbon blocks and fluorocarbon blocks results in a distinct polymorphism of these compounds, not yet fully understood.[5] Typically layered smectic structures are formed, in which interdigitation, tilting, and partial disordering of the alkyl chain segments account for the mismatch in the van der Waals diameters of the two blocks.[4,5,14,17]

* To whom correspondence should be addressed. Telephone: +49 (0) 241/80-233-30. Fax: 49 (0) 241/80-233-01. E-mails: mourran@dwi.rwth-aachen.de; Moeller@dwi.rwth-aachen.de.

† Universität Ulm.

‡ Current address: Lehrstuhl für Textilchemie und Macromolekulare chemie der RWTH Aachen, Worringer Weg 1, D-52056 Aachen, Germany.

§ Current address: Physics Department, Moscow State University, 119992 Moscow, Russia.

‖ Digital Instruments.

⊥ FOM-Institute for Atomic and Molecular Physics.

¶ DUBBLE CRG.

(1) Mahler, W.; Guillon, D.; Skoulios, A. *Mol. Cryst. Liq. Cryst. Lett.* **1985**, *2*, 111.

(2) Viney, C.; Russell, T. P.; Depero, L. E. *Liq. Cryst*. **1989**, *5*, 1783.

(3) Rabolt, J. F.; Russell, T. P.; Twieg, R. J. *Macromolecules* **1984**, *17*, 2786.

(4) Russell, T. P.; Rabolt, J. F.; Twieg, R. J.; Siemens, R. L.; Farmer, B. L. *Macromolecules* **1986**, *19*, 1135.

(5) Marczuk, P.; Lang, P. *Macromolecules* **1998**, *31*, 9013.

(6) Marczuk, P.; Lang, P.; Findenegg, G. H.; Mehta, S. K.; Moeller, M. *Langmuir* **2002**, *18*, 6830.

(7) Gaines, G. L., Jr. *Langmuir* **1991**, *7*, 3054.

(8) Huang, Z.; Acero, A. A.; Lei, N.; Rice, S. A.; Zhang, Z.; Schlossman, M. L. *J. Chem. Soc., Faraday Trans*. **1996**, *92*, 545.

(9) Krafft, M. P.; Giulieri, F.; Fontaine, P.; Goldmann, M. *Langmuir* **2001**, *17*, 6577.

(10) Maaloum, M.; Muller, P.; Krafft, M.-P. *Angew. Chem., Int. Ed.* **2002**, *41*, 4331−34.

(11) Krafft, M.-P. *Curr. Opin. Colloid Interface Sci.* **2003**, *8*, 243.

(12) Kato, T.; Kameyama, M.; Ehara, M.; Iimura, K. *Langmuir* **1998**, *14*, 1786.

(13) Gallyamov, M. O.; Tartsch, B.; Khokhlov, A. R.; Sheiko, S. S.; Börner, H. G.; Matyjaszewski, K.; Möller M. *Chem. Eur. J.* **2004**, *10*, 4599. See also: Gallyamov, M. O.; Tartsch, B.; Khokhlov, A. R.; Sheiko, S. S.; Börner, H. G.; Matyjaszewski, K.; Möller M. *J. Microsc.* **2004**, *215*, 245.

(14) Höpken, J. Fluorocarbon−Hydrocarbon Molecules, Structural Components for Self-Organizing Materials. Dissertation, University of Twente, Netherlands, 1991. Höpken, J.; Pugh, C.; Richtering, W.; Möller, M. *Makromol. Chem.* **1988**, *189*, 911.

(15) See, for example: Tolan, M. X-ray Scattering from Soft Matter Thin Films; Springer: Berlin, Germany, 1999.

(16) Gallyamov, M. O.; Mourran, A.; Tartsch, B.; Vinokur, R. A.; Nikitin, L. N.; Khokhlov, A. R.; Schaumburg, K.; Moeller, M. Manuscript in preparation.

10.1021/la048069y CCC: $30.25
Published on Web 02/10/2005

In ultrathin layers with a thickness comparable to the molecular length, it is expected that geometrical constraints imposed by the interfaces in combination with competing ordering of the building blocks will result in structures that differ significantly from the bulk smectic structure.[6,17] This issue has been addressed earlier in studies on Langmuir−Blodget[7] films. The interaction between the fluorinated segments was found to dominate the structure of the monofilm preserving the hexagonal close packing of the fluorinated segments.[8,9] It was reported that the hydrocarbon block formed a layer with a liquid-like order. When a Langmuir−Blodget monlayer of F_8H_{16} was transferred onto a silicon oxide surface, scanning force microscopy investigations showed that the layer consisted of monodisperse discrete aggregates. The formation of such structures has been explained by surface-induced aggregation, i.e., as "surface micelles", whose size is controlled by the density mismatch between the fluorinated and hydrogenated segments depending on their relative length.[10,11] Similar superstructures have been observed for partially fluorinated fatty acids on an aqueous subphase.[12]

Significant effort has been dedicated to elucidate the effect of the relative length of both blocks on the molecular conformation in a single layer, but no explanation has been found for the formation of the well-defined finite aggregates. Here we address this issue and report on the 2D assembly of molecularly thin films of eicosylperfluorotetradedcane, $F(CF_2)_{14}(CH_2)_{20}H$ (in brief $F_{14}H_{20}$), on silicon/SiO_2, mica, and water. We focus on whether and how the self-assembled structures are influenced by the choice of the solvent from which the films are deposited. Scanning force microscopy (SFM) was employed to depict the morphologies. X-ray reflectivity was used to measure the film thickness and to probe the laterally averaged electronic density normal to the solid interface. A new model is proposed for the molecular structure of the self-assembled objects. One of the more interesting results obtained from this study is the ability to convert the aggregates from one morphology to another if exposed to solvent vapors of different nature. These transformations have been observed in situ by SFM and are believed to be caused partly by selective uptake of the solvent within the aggregates, but also partly by coadsorption of the solvent at the substrate resulting in a modification of the adhesive interaction of the semifluorinated alkanes.[13]

2. Experimental Section

Materials and Preparation. The $F_{14}H_{20}$ sample was synthesized according to the procedures reported elsewhere.[14] Three types of solvents were used: selective solvents for either the fluorinated blocks (perfluorodecalin, perfluorohexane) or for the hydrocarbon blocks (decalin, xylene, isooctane, chloroform), and a solvent that is able to dissolve both parts of the molecule (hexafluoroxylene). Decahydronaphthalene (decalin; Merck; 98%, mixture of cis and trans), perfluordecalin (Aldrich; 95%, mixture of cis and trans), and 1,3-bis(trifluoromethyl)benzene (hexafluoroxylene, HFX; Apollo Scientific) have been used as received.

Solutions of $F_{14}H_{20}$ with concentrations of 1 and 0.1 g/L were prepared. To ensure complete dissolution of the compound, the solutions were heated to 120 °C for 30 min and subsequently the flasks were put aside to cool to room temperature. When decalin was used as a solvent, dilution of the solution was necessary to avoid gel formation. In the case of perfluorodecalin or perfluorohexane, dilution was necessary to avoid precipitation. HFX dissolves the compound without formation of precipitates.

Freshly cleaved mica or cleaned silicon wafers were used as substrates. Monomolecular layers were prepared either by transfer of a Langmuir−Blodgett (LB) film or by spin coating. The LB experiments have been performed on a Lauda FW2 Langmuir through with a surface area of 927 cm^2 operated at 22 °C using Milli-Q water as subphase. A defined volume of the solution was deposited at the air−water interface. Compression of the monolayers started after a 2−4 h delay to ensure homogeneous spreading of the solution and complete evaporation of the solvent. During compression, the surface area was reduced by 5%/min. Transfer on the substrate followed at constant surface pressure by lowering the subphase. In the spinning procedure, 2000 rpm was found to produce a monolayer that covered the substrate homogeneously.

Scanning force microscopy (SFM) was performed using the following devices:

a Digital Instruments Multimode scanning force microscope equipped with a Nanoscope IIIa controller. Imaging was done in the tapping mode using standard silicon cantilevers: Nanoworld Pointprobe NCH ($k \approx 42$ N/m, $f_0 \approx 330$ kHz) or FM ($k \approx 2.8$ N/m, $f_0 \approx 70$ kHz).

A molecular Imaging PicoSPM scanning force microscope equipped with a Digital Instruments Nanoscope IIIa controller and an environmental chamber, which allows imaging under controlled vapor atmosphere. The scanning was done in the acoustic mode using standard silicon cantilevers: Nanoworld Pointprobe FM (k ≈ 2.8 N/m, $f_0 \approx 70$ kHz).

X-ray Reflectivity. The films were investigated by specular X-ray reflectivity carried out at beam line BW2 of HASYLAB (DESY, Hamburg, Germany) at an energy of 10 keV, corresponding to a wavelength $\lambda = 0.124$ nm. At specular reflectivity the momentum transfer $q = k_{out} - k_{in}$ is perpendicular to the film (z-direction), i.e., $|q| = q_z = (4\pi/\lambda)\sin\theta$, where 2θ is the scattering angle. Hence the reflected intensity is sensitive to the electron density profile in the latter direction, averaged over the footprint of the incident beam. The resolution was set at $\Delta q_z = 0.025$ nm^{-1}. The density profile was determined by comparing the calculated and the experimental reflectivity.[15] Calculations were based on the Parratt algorithm using a parametrized molecular model in which two sublayers were approximated by a boxlike function characterized by thickness and density, convoluted with a Gaussian probability describing the interfacial roughness. The best-fit curve to the data was determined by a minimization procedure leading to a density and roughness profile along the film normal. The total thickness was directly determined by the interference oscillations (Kiessig fringes) between X-rays reflected from the top and bottom of the film, which is in principle model-independent.

Grazing-incidence X-ray diffraction (GIXD) was performed both at beam line BW2 of HASYLAB at 10 keV and at BM26 (DUBBLE) of the ESRF (Grenoble, France). In the latter case the energy was 15.9 keV, leading to $\lambda = 0.0779$ nm. In GIXD the X-ray beam is incident at the surface of the sample at a small glancing angle below the critical angle of total reflection. Under these conditions only an evanescent wave is generated that propagates along the film−air interface and penetrates into the film with an intensity exponentially decaying with depth. The evanescent wave can be considered as incident beam for 2D X-ray diffraction, giving information about the 2D structure in the plane of the film. The incident angle was set between the critical angles of the $F_{14}H_{20}$ monolayer and the substrate, respectively, resulting in 2D diffraction from the complete monolayer. The overall resolution in the sample plane was set to 0.01 nm^{-1}. The scattered intensity was recorded at different out-of-plane angles using a scintillation detector.

3. Results and Discussion

3a. Scanning Force Microscopy. Figure 1a shows a SFM image of a monomolecular layer of $F_{14}H_{20}$ cast from a solution of HFX onto mica. The image depicts a hexagonal assembly of spiral nanoobjects (see Figure 1a). The spirals have an average diameter of 80 ± 5 nm and consist of short ribbons with a width of 35.0 ± 3.0 nm and a height of 3.0 ± 0.5 nm (determined by SFM) that are bent rather sharply at distances of 30−60 nm by an angle of 105−130°. Within each spiral these kinks turn in the same direction, but the different spirals are both right- and

(17) Gang, O.; Ellmann, J.; Möller, M.; Kraack, H.; Sirota, E. B.; Ocko, B. M.; Deutsch, M. *Europhys. Lett.* **2000**, *48* (6), 761.

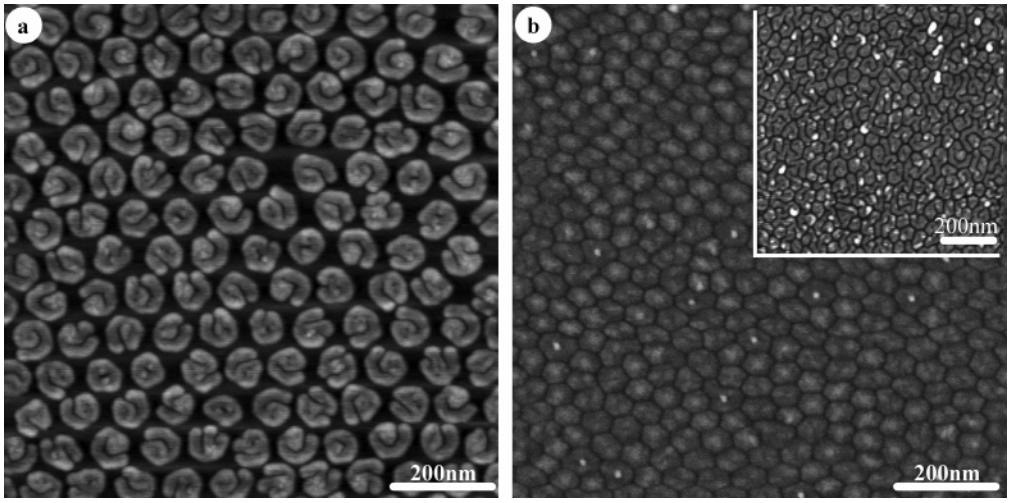

Figure 1. SFM tapping-mode topography images of $F_{14}H_{20}$ prepared from HFX solution (1 g/L) on mica by (a) spin coating (2000 rpm) and (b) by LB-film deposition transferred at a surface pressure of 4.9 mN/m. The insert shows the same sample after 13 days at room temperature.

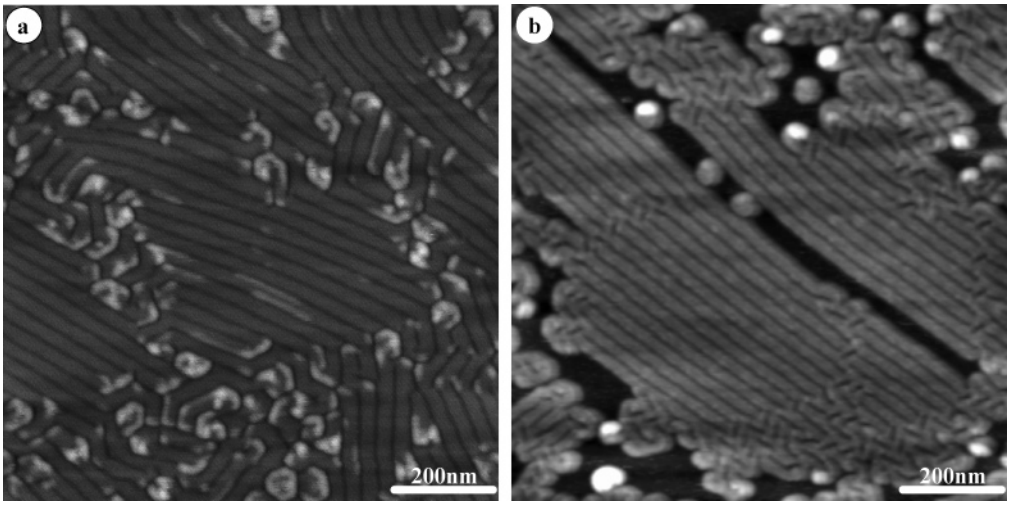

Figure 2. SPM tapping-mode topography images of $F_{14}H_{20}$ prepared from decalin solution on mica by (a) spin coating (2000 rpm), $c = 1$ g/L and (b) LB-film preparation, spread from decalin solution with a concentration of 0.1 g/L and transferred at a surface pressure of 4.6 mN/m.

left-handed, showing no preference in chirality. As discussed below, we have tested various solvents; however, so far only HFX and supercritical carbon dioxide[16] lead to the formation of the nanospirals.

To address the effect of the preparation method on the morphology, a defined volume of the solution was deposited at the air−water interface on a Langmuir trough. After complete evaporation of the solvent, the monofilm was compressed up to 4.9 mN/m; the corresponding surface area per molecules is 0.24 nm^2, which is 30% smaller than the mean area of similar semifluorinated alkanes at the bulk surface.[17] For SFM, the floating film was transferred onto mica or onto a silicon wafer. Figure 1b depicts a two-dimensional assembly of uniformly sized spirals with a mean periodicity of 60 nm. The comparison of the SFM images in Figure 1 demonstrates for the LB film a high coverage of the substrate compared to the spin-coated film. Lateral compression of the self-assembled objects yields faceted-edged hexagonal toroids, with a size comparable to the original spirals. The closed ring structure can open again to spirals, as it is not stable as shown in the inset of Figure 1b that depicts the sample after it was stored several days at room temperature. The same structure was observed when silicon wafers were used as a substrate. We conclude that neither the substrate nor the preparation method (LB film versus spin-coated film) influence winding up of the ribbons to spirals. However, lateral compression of the monofilms demonstrated significant elasticity of the shape of the nanoobjects. The effect of compression on the structure of the monolayer is beyond the scope of this paper. Somewhat similar structures have been observed by Kato et al. for partially fluorinated long-chain acids.[12]

When a homogeneous layer of $F_{14}H_{20}$ was prepared on mica by spin coating from decalin solution, a rather preferential solvent for the hydrocarbon block straight ribbons were observed (Figure 2a). This morphology is even more clearly developed in Figure 2b, which depicts a film on mica prepared by LB deposition. The transfer was achieved at a surface pressure of 4.6 mN/m corresponding to an area per molecule of 0.24 nm^2. Compared to LB deposition, the spin-coating process yielded a more homogeneous coverage of the surface. Both samples demonstrate the coexistence of spiral structures with ribbons. The height and the width of the ribbons have been measured by SFM to be 3.0 ± 0.5 nm and a width of 35 ± 3 nm respectively, i.e., identical to the corresponding values of the spirals formed from HFX solution.

Straight ribbons were also observed when monofilms were prepared with a fluorinated solvent that is rather selective for the fluorinated block. Figure 3a shows the

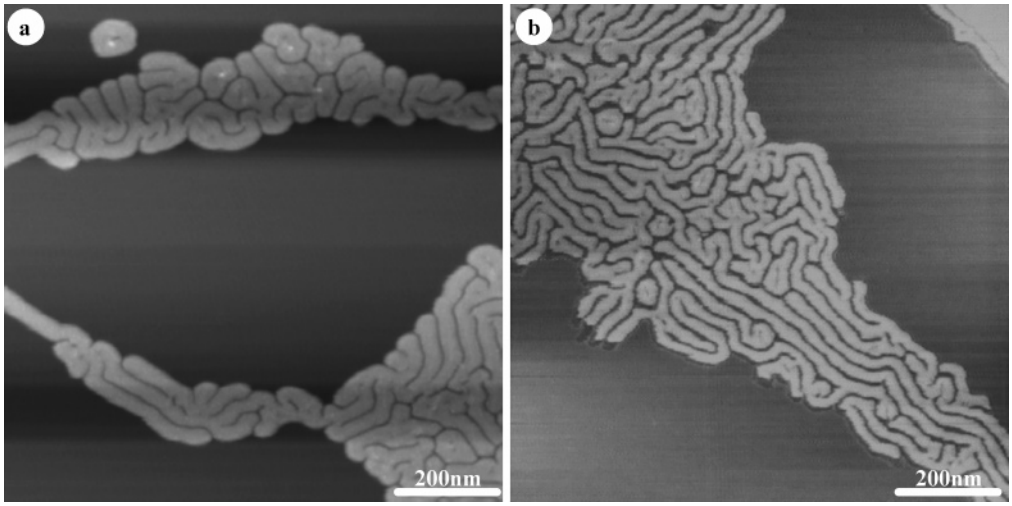

Figure 3. SPM tapping-mode topography images of $F_{14}H_{20}$ prepared from (a) perfluorohexane solution (c = 0.1 g/L) on mica by spin coating (2000 rpm) and (b) perfluorodecalin solution (c = 0.1 g/L) on mica by spin coating (2000 rpm).

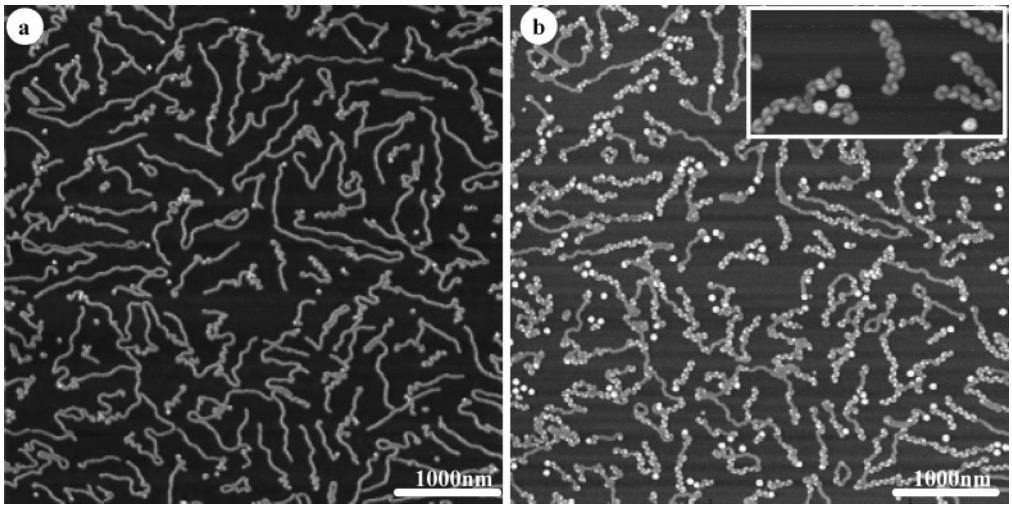

Figure 4. (a) As-cast film from 0.1 mg/mL solution of decalin at 2000 rpm and (b) after exposure to HFX vapor during 20 h.

morphology of the spin-cast film from dilute solution of perfluorohexane; Figure 3b, a spin coated monofilm prepared from perfluorodecalin. The low coverage of the surface is due to the high dilution of the solution, which was necessary to prevent precipitation. The height and the width of the ribbons as determined from SFM are the same as those for the other samples, i.e., 3.0 ± 0.5 nm and 35 ± 5 nm, respectively. However, the ribbons exhibit a stronger tendency to bend than in hydrogenated solvent (Figure 2). In some areas of the sample, even isolated spirals are depicted as observed exclusively for the HFX preparation.

So far, it is not clear whether the spirals/toroids are preformed by crystallization in solution and to which extent the formation of the observed structures is effected by the contact with the substrate. To answer this question, the samples were exposed to the vapor of the corresponding solvents and the resulting structural transformations were observed by SFM in situ.

Results are displayed in Figure 4. Two snapshots have been selected that capture the main features of the structural transformation. Figure 4a shows the surface morphology of the as-cast sample from decalin solution. Well-isolated ribbons were obtained. Figure 4b shows the same area of the sample after treatment with HFX vapor during 20 h. The micrograph demonstrates a transition from straight ribbons to bent ribbons and spirals. The inset in the image (top-right corner) magnifies the bent, meander-like structures. These results demonstrate explicitly the effect of the solvent on the structure. As an explanation we propose that the solvent molecules get coadsorbed at the substrate surface and this way the interaction of the semifluorinated alkane layer with the substrate is eased, allowing the transformation to the spirals/toroids. Such an explanation would be consistent with the assumption that the donuts are formed while the solvent molecules prevent the directing interaction of the surface with the crystallizing molecules.

When we treated a sample that consisted predominantly of nanospirals/toroids with the vapor either of decalin or perfluordecalin, we observed the reverse transformation. For the images in Figure 5, the initial state was chosen as the spiral morphology cast from a dilute HFX solution (Figure 5a). While the surface was scanned at optimum imaging conditions, perfluorodecalin vapor was generated in the SPM chamber. Figure 5b shows straight ribbons that developed within 20 h vapor treatment. Even though some of the spiral structures persisted, the morphological transformation triggered by the solvent vapor is obvious. When a similar HFX born sample was exposed to decalin, transformation of the well-defined nanospiral to straight ribbons was observed only in the scanning area (not shown). In general the observation is consistent with the explanation that the vapor molecules help to introduce

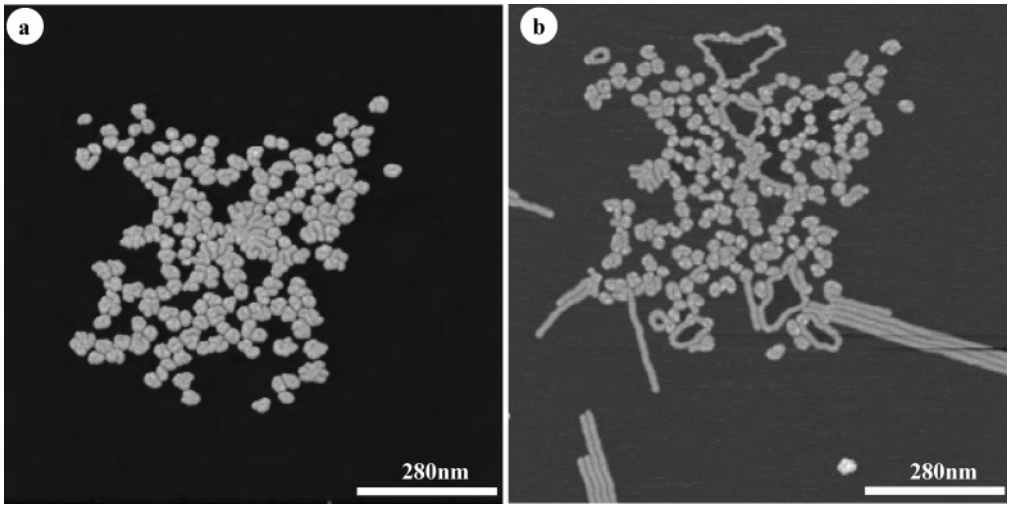

Figure 5. (a) As-cast film from 0.1 mg/mL solution of HFX at 2000 rpm and (b) after exposure to perfluorodecalin vapor during 20 h.

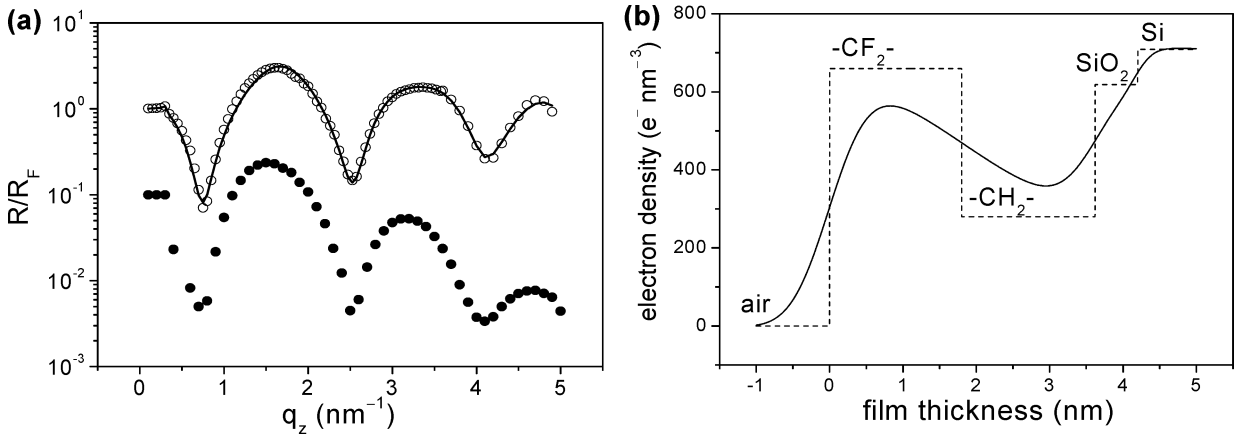

Figure 6. X-ray reflectivity results from a $F_{14}H_{20}$ monolayer (thickness, 3.6 nm). (a) Intensity normalized to the Fresnel reflectivity for a ribbon (top) and a spiral sample (bottom). The latter has been shifted by a decade for clarity. (b) Electron density profiles corresponding to the fit of the ribbon data, with (full line) and without (dashed line) roughness included.

some mobility but, most importantly, effect the modification of the structure by coadsorption.[13] Perfluordecalin interacts very weakly with the substrate and does not shield the alkyl chains from interaction with the mica. Decalin gets adsorbed as an interlayer, but in this case the reorganization has to be promoted by the mechanical stimulus of the scanning tip.

Although the explanation remains somehow speculative, it may be summarized that, in all cases, the structures could be converted from spirals or meanders of a characteristic size to straight ribbons and vice versa, while the height and width of the bands were conserved.

3b. X-ray Reflectivity. To obtain further insight into the structure of the monolayers, X-ray reflectivity (XR) and grazing incidence X-ray diffraction have been used. The former allows to derive the thickness and the density distribution along the normal to the interfaces. The latter gives direct evidence about the in-plane packing of the semifluorinated chain molecules.

Monolayers of $F_{14}H_{20}$ were prepared from low-concentration solutions in different solvents on a silicon substrate by transferring a closed film of the sample from the surface of water on a LB trough. The LB technique was chosen to ensure optimum coverage of the surface. SFM was used to control the quality of the transfer and only samples with a complete monofilm (coverage > 90%) were investigated by XR. Figure 6a shows the reflected X-ray intensity of a film with both spirals and ribbons. The ribbon sample was fitted in detail to a two-layer model, which resulted in the density profile of Figure 6b. The corresponding fitting parameters are given in Table 1. The smaller density of the bottom layer unambiguously puts the hydrogenated part of the molecules near the surface. The single-frequency oscillations indicate a uniform thickness. From the fit of the interference fringes this film thickness was derived to be 3.6 ± 0.05 nm, which exceeded the SFM data by 20%. The discrepancy can be attributed to a certain indentation of the SFM tip into the soft $F_{14}H_{20}$ film upon tapping, resulting in height values that are systematically too small. Thus the X-ray value must be taken as the correct layer thickness. This value is smaller than the length of the extended molecule, i.e., 4.65 nm (1.98 + 0.126 × 20 + 0.15) nm, where 1.98 nm is the length of the F block[18]). It is, however, consistent

Table 1. Summary of the XR Fitting Results (d_{calc} Is According to the Close-Packed Model of Figure 7)

	$d_{fit} \pm 0.05$ (nm)	d_{calc} (nm)	$\rho_{fit} \pm 10$ ($e^- nm^{-3}$)	$\rho_{lit.}$ ($e^- nm^{-3}$)	$\sigma \pm 0.05$ (nm)
$F(CF_2)_{14}$	1.80	1.98	660	670	0.42
$H(CH_2)_{20}$	1.82	1.41	280	320	1.20
SiO_2	0.58		fixed	618	0.39
Si	∞		fixed	708	0.18

(18) Lo Nostro, P. L.; Ched, S.-H. *J. Phys. Chem.* **1993**, *97*, 6535.
(19) Daillant, J.; Gibaud, A. *X-ray and Neutron Reflectivity: Principles and Applications*; Springer: Heidelberg, Germany, 1999.

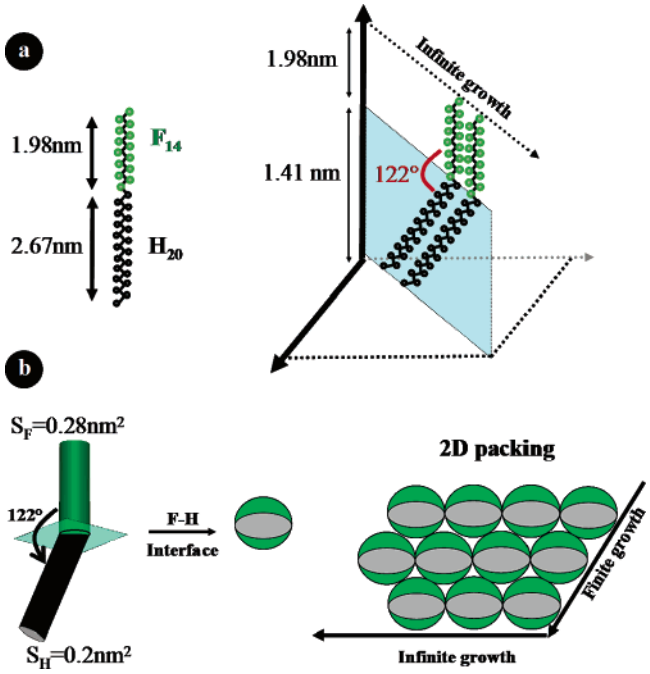

Figure 7. (a) Molecular dimensions of $F_{14}H_{20}$ and model with tilted hydrogenated chains. (b) Illustration of infinite growth along the (easy) tilted direction and finite (frustrated) growth perpendicular to the tilt plane. SF and SH are the cross-sectional areas of F and H, respectively.[5,20]

with a monolayer with a tilt angle of 127° at the linkage between the fluorocarbon and the hydrocarbon segments. Geometrical considerations demonstrate that a tilt of 122° will allow closed packing of the chains in the plane defined by the zigzag band of the all-trans planar $(CH_2)_n$ segment, this way compensating for the larger cross-section area of the fluorocarbon segment compared to the extended hydrocarbon tail within this plane (see Figure 7). The van der Waals diameters of the fluorocarbon and hydrocarbon parts are 0.6 and 0.48 nm, respectively. This results because a -$(CF_2)_n$- sequence cannot exist in a planar zigzag configuration, as is possible for -$(CH_2)_m$-. Instead the -$(CF_2)_n$- sequence adopts a 15/7 helix, leading to a rigid rodlike structure. The apparent tilt angle of 127° corresponds to a reduction of the length of the hydrocarbon chain by 0.2 nm by contribution of gauche conformations along the -$(CH_2)_m$- segment caused by the mismatch of the cross-section of the constituting segments.

The densities of the two parts of the monolayer deserve some more discussion. In the fitting procedure the densities of the substrate (silicon plus an oxide layer) are kept fixed at their literature values (Table 1). The top-layer density is in good agreement with the calculated one for fluorocarbons using literature data.[19] The somewhat lower value can be attributed to the coverage of the surface, which is less than 100%. However, in the fitting procedure the densities of the sublayers couple strongly to their thickness. As moreover the minimum is very shallow, this leaves some ambiguity. Therefore we have chosen to fix the densities according to the closed-packed model, taking for the fluorinated top layer a density slightly below the literature value, and correct for the bottom layer the hydrocarbon literature values for the loose packing in the direction perpendicular to the easy axis, i.e., the ribbons. The values in Table 1 are the result of this procedure. Incorporation of roughness σ of the interfaces in the model (see Figure 6b) effectively partly mixes the two different parts, leading to some averaging of the densities. The values of σ of the top and bottom

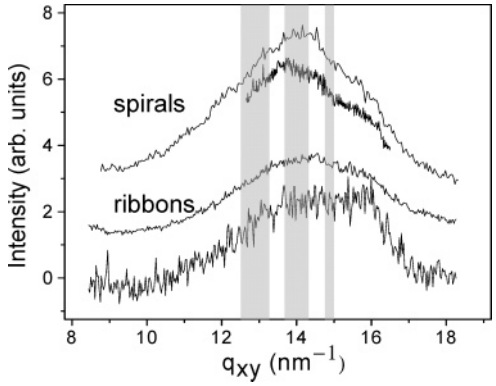

Figure 8. Summary of the GIXD results on $F_{14}H_{20}$ monolayers at ESRF, indicating composite liquid peaks. The gray bands indicate the q-range of literature data of (from left to right) hexagonal packed fluorocarbons, liquidlike ordered hydrocarbons, and close-packed hydrocarbons, respectively.

interfaces are as usual for soft films, but the value of the middle interface is rather large. It is difficult to imagine large density variations at this interface without the other ones also being affected. We take this large roughness as further evidence of a transition region. Hence, it seems that a three-layer fit to the XR data could be more appropriate. We did not pursue such an exercise because of the associated increase in the number of parameters.

3c. Grazing-Incidence X-ray Diffraction. The major results from GIXD of ribbon and spiral monolayers are summarized in Figure 8. Note that these results effectively correspond to 2D "powder"-averaged intensities. Hence, the azimuthal orientation should not make any difference. For all samples we find a broad composite in-plane liquidlike peak that comprises the range of crystalline and liquid fluorocarbon and hydrocarbon (lattice) spacing d_{10}. Note that upon crystallization, the spacing of fluorocarbons hardly changes, contrary to the situation in hydrocarbons. In the latter case the closed-packed value does not necessarily correspond to full crystallization as also intermediate solid-rotator phases can play a role.[20] Figure 9 gives details of the fitting of the upper curve from Figure 8 to either two or three Lorentzians. From the quality of the fits (note the shoulder at the right) we conclude that the representation by three liquid peaks is significantly superior to the two-peak fit. Similar results are found for the ribbon samples (not shown). The final results are given in Table 2, where $d_{10} = 2\pi/q_{xy}$ and Δq_{xy} is given as the full width at half-maximum (fwhm) with the correlation length as $\xi = 2/\Delta q_{xy}$. The value of ξ indicates the range of ordering associated with the peak and extends to a few molecular lengths, which is quite normal for liquid order. Summarizing the results so far, we conclude that both the alkylated and the fluorinated parts are largely in a liquidlike state. Several liquidlike peaks have been observed, and within the experimental accuracy the fits indicate q-values close to the three types of ordering indicated in Figure 8. The dominant fluorcarbon top layer can be considered as a single smectic-A layer with liquid in-plane ordering. Evidently any tendency to crystallize—anticipated because of a bulk melting point well above room temperature—is in these monolayer samples strongly suppressed.

(20) Ocko, B. M.; Wu, X. Z.; Sirota, E. B.; Sinha, S. K.; Gang, O.; Deutsch, M. *Phys. Rev. E* **1997**, *55*, 3164.
(21) Fera, A.; Dolbnya, I. P.; Opitz, R.; Ostrovskii, B. I.; de Jeu, W. H. *Phys. Rev. E* **2001**, *63*, 020601.
(22) Ostrovskii, B. I. *Structure and Bonding, Liquid Crystals I*; Springer: New York, NY, and Heidelberg, Germany, 1999; Vol. 94, p 199.

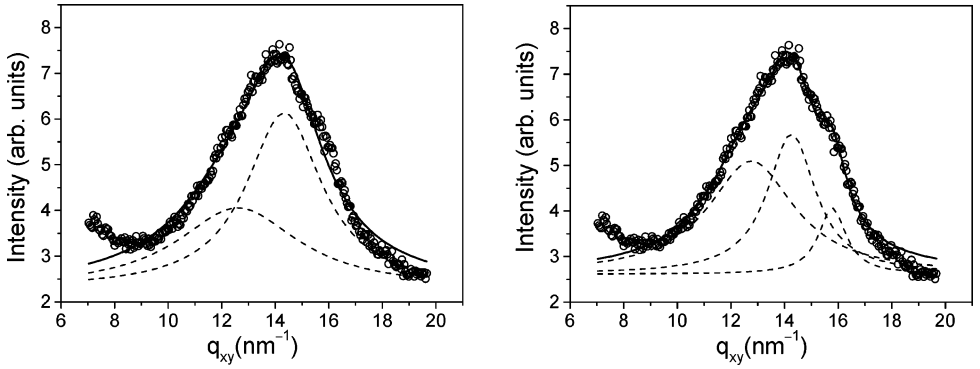

Figure 9. GID data (circles) from the amorphous $F_{14}H_{20}$ monolayer with the spiral morphology of Figure 8. The full lines are the sum of two (left) and three (right) Lorentzian peaks, respectively.

Table 2. Summary of the Three-Lorentzian GID Fitting Results from the Amorphous Monolayers (ESRF)

sample type	$q_{xy} \pm 0.1$ (nm^{-1})	$d_{10} \pm 0.05$ (nm)	$\Delta q_{xy} \pm 0.05$ (nm^{-1})	$\xi \pm 0.1$ (nm)
ribbon	13.4	0.47	3.3	0.6
	14.9	0.42	2.0	1.0
	15.9	0.39	0.9	2.3
spiral	12.8	0.49	3.9	0.5
	14.3	0.44	2.2	0.9
	15.8	0.40	1.2	1.6

At a later stage we studied a new series of samples at HASLAB and found the rather different behavior indicated in Figure 10. In contrast to the previous series, a crystalline peak now dominates the in-plane diffraction. The fitting results for the central Gaussian crystalline peaks are given in Table 3 with the width given by $L = 2\pi/\Delta q_{xy}$. From the observed spacing we conclude that the fluorcarbon top layer is involved in the crystallization. The finite width of the crystalline peak agrees well with the transverse size of the ribbons. Figure 11 shows a 2D contour plot of the X-ray intensity in the (q_z, q_{xy})-plan, indicating clearly that the fluorcarbon chains in the crystalline layer are not tilted. We emphasize that for this second series of samples the morphology as seen in atomic force microscopy (AFM; studied both before and after the X-ray measurements) is not different from the earlier series. The only different aspect of the sample treatment is transport between Aachen and Amsterdam in July for the first series (summer) and in December for the second one (winter). Hence, we assume that crystallization has occurred in the second series by exposure to lower temperatures during transport.

The final conclusions from the GIXD experiments can be summarized as follows. (i) The nontilted fluorcarbon top layer determines the morphology both for ribbons and spirals. (ii) Whether this top layer is smectic (liquid in-plane order) or crystalline appears to be of minor importance. At first sight the latter point might be surprising. However, from free-standing smectic liquid crystalline films it is known that, for thin films up to several tens of layers, there is hardly any difference in physical behavior between smectic-A films with liquid layers and crystalline-B films in which the layers are crystallized.[21] In both situations the film properties are surface-dominated because it takes many layers to build up the 3D structure for which shear elasticity starts playing a role. Transferring this knowledge to the present situation, there is no reason to expect much difference between a liquid and a crystallized fluorinated single smectic layer.

To put the results so far in a broader context, we first note that F_nH_m compounds in their high-temperature bulk solid phase are commonly arranged in monolayer lamellar stacks. In these stacks the fluorinated chains are oriented vertical to the planes of the 2D close packing, while the hydrocarbon tails are in a weakly ordered liquidlike state with a large number of gauche defects along the chain.[5] This type of structure is retained in the monolayers found at surface freezing of semifluorinated alkane melts $F_{12}H_m$ above the bulk freezing point,[17] at least for the shorter H-blocks. For $F_{12}H_{18}$ (which is close to our sample) only short-range in-plane order was observed. GIXD of monolayers of $F_{12}H_{18}$ at the air−water interface indicated hexagonal closed packing, though this equilibrium was only reached after appreciable time.[8] From these results it seems that our $F_{14}H_{20}$ system is close to a transition region (in terms of the respective block length) for which the monolayers "hesitate" to crystallize. This explains at least partly the difference in behavior between series 1 (composite liquid in-plane order) and series 2 (crystallized fluorocarbon layers). Another factor contributing to suppression of crystallization is probably the confined structure of the ribbons. In series 2 this lateral confinement is expressed as finite-size broadening of the crystalline peaks of the fluorinated layers.

Let us now consider the basic elements of the ribbon structure. The possibility of a tilted arrangement of the hydrogenated part with respect to the fluorinated part of the molecules has so far received little attention in the vast literature about fluorinated alkanes.[11] However, as mentioned above, this optimum packing can only materialize in one plane, leading to an "easy" long direction that in principle explains the ribbonlike structures (see Figure 7). Perpendicular to the easy direction, the frustration due to the difference in van der Waals radii of the fluorinated and hydrogenated parts is not released. In Figure 12 two extreme possible models are sketched for the structure of a cut perpendicular to the long direction of a ribbon. In model I the fluorocarbon parts of the molecules are assumed to interact strongly and to form a single smectic or crystalline layer. The hydrocarbon parts have to adapt to this situation, leading to a frustrated bottom layer. Along the long direction of the ribbons the hydrocarbon parts are close-packed. This allows only little freedom to coil in the frustrated direction. The chains can mainly tilt and perhaps coil somewhat in order to optimize the packing. As a result only a limited width of fluorinated layer can be supported, which will end abruptly. Evidently this leads to an approximately constant width, which should vary with the length of the alkyl chains. Model II can be considered as the other extreme, in which the molecules are assumed to be effectively wedge-shaped. It assumes that the packing of the hydrocarbon part dominates and that the thicker fluorocarbon part follows.

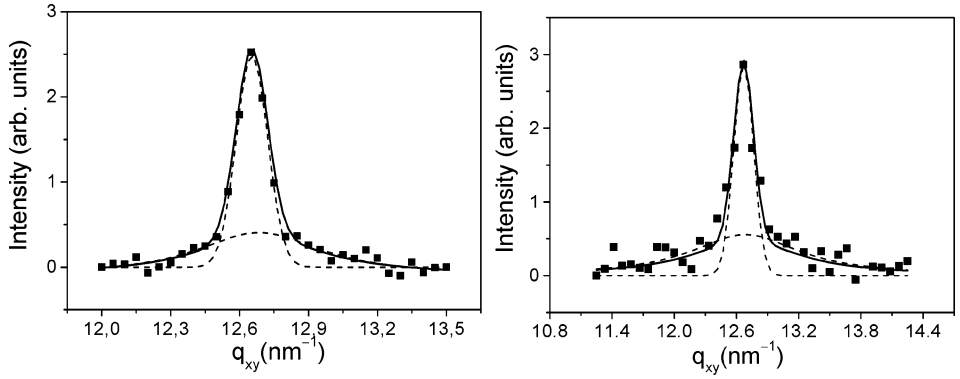

Figure 10. GID data (Hasylab)) from crystallized $F_{14}H_{20}$ monolayers with donut (left) and ribbon (right) morphology (solid squares). The full line gives a fit to a Gaussian diffraction peak and a Lorentzian amorphous background (broken lines).

Table 3. Summary of the Gaussian GID Fitting of the Crystallized Monolayers (Hasylab)

sample	$q_{xy} \pm 0.01$ (nm^{-1})	$d_{10} \pm 0.05$ (nm)	$\Delta q_{xy} \pm 0.05$ (nm^{-1})	$L \pm 0.5$ (nm)
ribbon	12.6	0.49	0.19	33
spiral	12.6	0.49	0.14	46

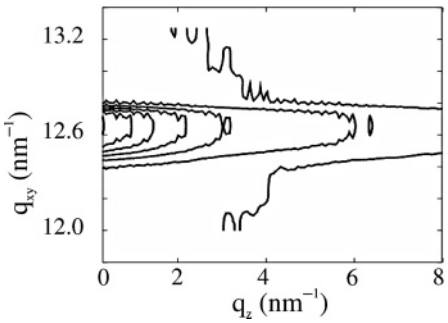

Figure 11. Two-dimensional contour plot of the GIXD intensity of crystallized $F_{14}H_{20}$ monolayers with spiral morphology.

Such packing is known for some smectic phases of liquid crystalline molecules.[22] It will lead to a continuous curvature of the upper surface, evidently also leading to a constant width.

Considering the situation in detail there is considerable evidence in favor of model I:

(1) In X-ray reflectivity relatively pronounced minima are observed, indicating a well-defined structure of layers. In the case of a strong curvature (model II) a parallel X-ray beam would experience a broad distribution of incident angles. In that situation, there is no well-defined thickness and no Kiessig fringes would be observed in the X-ray reflectivity. In fact the minima disappear at an angular spread larger than about 0.1°. Hence, this number puts an upper limit to curved regions that still contribute to the distinguishing features of the reflectivity curve. Kraft et al. reached a similar conclusion for monolayers of F_8H_{16} for which a top interface with an ellipsoidal curvature could not fit their data.[10]

(2) The densities of the two layers as observed in XR agree well with the calculated values. This is not expected for model II, which would give an increased density of the bottom layer due to the bended fluorocarbon parts.

(3) GIXD of $F_{14}H_{20}$ indicates that the fluorinated parts of the molecules are arranged perpendicular to the surface in a layered structure. Depending on temperature and history the -$(CF_2)_n$- layer is either crystallized or smectic (liquidlike), which does not make much of a difference for the present discussion. In agreement with this statement the AFM morphologies are in both cases very similar.

In model I the constant width in the frustrated direction should depend on the length of the CH_2 parts. Indeed we observed for various choices of the CF_2 length that the width increases with m_H, the number of CH_2 groups. A larger value of m_H is indeed expected to allow a larger variation of CH_2 conformations, and thus more possibilities to support the CF_2 layer.

We conclude that model I for the finite width of the ribbons will be close to the cartoon model I of Figure 12. Of course it should be realized that a realistic model will not be as extreme as pictured and can be expected to contain local differences in structure.

Finally we come to a discussion of ribbons versus spirals. From the results so far it seems that the ribbon pattern is the natural way to accommodate a monolayer of $F_{14}H_{20}$. This is conclusively explained by the difference between the closed packing along the ribbons and the frustrated packing in the transverse direction. The latter leads to a constant width that is preserved in the spiral structure as well. Note that spirallike patterns have been reported earlier in monolayers, but have usually been treated as hemispherical micelles.[10] In the present case of $F_{14}H_{20}$, the resolution of the SFM micrographs unambiguously depicts turning of short ribbons, schematically illustrated in Figure 13. This observation is quantitatively supported by the finite width of the crystalline peaks in Figure 10 (see also Table 3). In fact both right-handed and left-handed structures are found. Figure 4 shows ribbons where the turns alternate from right to left and vice versa (meander-like structures). Yet, Figure 1 is one of many examples where no change of rotation direction is observed within the spiral. Starting from the ribbon structure, we note that the kinks along the ribbon direction can be directed either forward or backward. A transition from one direction to the other leads to a defect. The stresses in packing near such a defect can be released by creating a discrete angular step along the ribbon, leading to a change in the azimuthal tilt angle direction. In the absence of any preference for a right or a left turn this is exactly as observed in the meandering structure of Figure 4. It needs a preference to continue in the same direction after the first turn, to explain the spirals of Figure 1. Note that the first azimuthal step can be directed either clockwise or counterclockwise, which explains the two types of spirals. At present it is not clear to us why a certain angular direction is continued and why the nanospirals can be obtained so easily with narrow size distributions as shown in Figure 4. We would like to speculate that the spirals grow at the air−solution interface at the outer end and wind up in the center where they finally cannot grow further due to the steric constraint. This might also explain

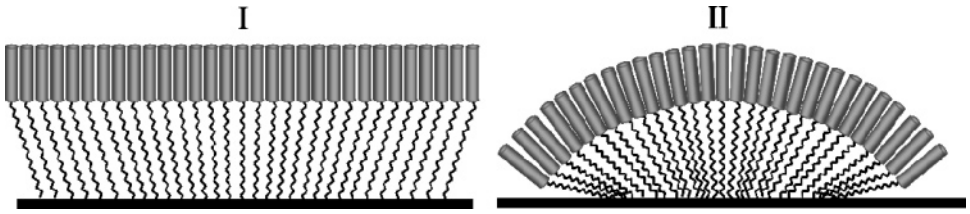

Figure 12. Cartoon of two extreme possibilities for the organization of $F_{14}H_{20}$ ribbons in the frustrated direction.

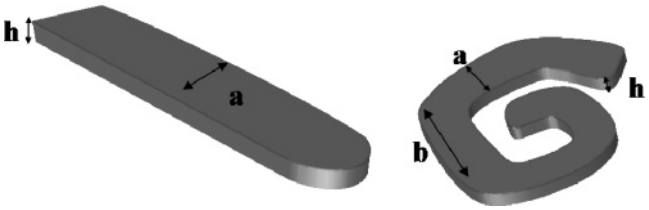

Figure 13. Schematic pictures of the ribbon and the spiral morphology.

why we find closed toroids only sometimes and why spirals can be compressed and open again.

Conclusion

We have demonstrated that a combination of SFM and surface X-ray scattering (XR and GIXD) provide detailed insight into the structure of supported monolayer of $F(CF_2)_{14}(CH_2)_{20}H$. We have shown that a single molecular layer of $F(CF_2)_{14}(CH_2)_{20}H$ on a solid substrate is laterally structured. SFM revealed two morphologies, i.e., straight ribbons and nanospirals. Whether the one or the other formed depended on the solvent from which the sample was prepared. Most strikingly, morphological transformation was observed in situ when samples were exposed to vapors of different solvents. Tentatively we explained the transformation by coadsorption of the solvent that moderates the interaction of the semifluorinated alkanes with the substrate.

The characteristic dimensions of both morphologies are identical, which suggests that the difference resides in the molecular packing. XR analysis confirmed that the height of the structures is less than the extended length of the molecules and revealed the layered structure of the monolayer. As GIXD proves that the fluorinated segments tend to pack with a chain orientation normal to the layer in an arrangement that would allow large 2D films, all the observed peculiarities in the morphology must be caused by ordering of the hydrocarbon chains. We have proposed a model with tilted hydrocarbon chains resulting in an easy axis that explains qualitatively the ribbon structure and the origin of the nanospirals. In the direction perpendicular to the easy axis the mismatch of dense packing of CF_2 and CH_2 groups can be released by partial disordering of the alkyl chains corresponding to an interlayer. Yet this incommensurability can only be compensated over a restricted length. These arguments give a first coarse indication for the formation of stripes or bands of uniform width. In one direction the incommensurability is compensated by the tilt of the hydrocarbon chain toward the normal of the monofilm; in the other direction it can be compensated only for a limited length by partial disordering of the hydrocarbon segment. Systematic investigations of the morphology as a function of the respective block lengths will be reported in a series of following publications.

Acknowledgment. The work at the FOM-Institute for Atomic and Molecular Physics is part of the research program of the "Stichting voor Fundamenteel Onderzoek der Materie (FOM)", which is financially supported by the "Nederlandse Organisatie voor Wetenschappelijk Onderzoek (NWO)". This work was partly funded by EU Project POLYNANO under Contract HPRN-CT-1999-00151 and with DIP Project A 1.3.

LA048069Y